REPORT DOCUMENTATION PAGE

Form Approved OMB NO. 0704-0188

1. REPORT DATE (DD-MM-YYYY)	2. REPORT TYPE	3. DATES COVERED (From - To)
	New Reprint	-

4. TITLE AND SUBTITLE

Understanding anion transport in an aminated trimethyl polyphenylene with high anionic conductivity

5a. CONTRACT NUMBER	W911NF-10-1-0520
5b. GRANT NUMBER	
5c. PROGRAM ELEMENT NUMBER	611103
5d. PROJECT NUMBER	
5e. TASK NUMBER	
5f. WORK UNIT NUMBER	

6. AUTHORS

James L. Horan, Benjamin R. Caire, Rajeswari Janarthanan, Zachary C. Ziegler, Yuan Yang, Xiaobing Zuo, Matthew W. Liberatore, Michael R. Hibbs, Andrew M. Herring

7. PERFORMING ORGANIZATION NAMES AND ADDRESSES

Colorado School of Mines
Colorado School of Mines
1500 Illinois Street
Golden, CO 80401 -

8. PERFORMING ORGANIZATION REPORT NUMBER

9. SPONSORING/MONITORING AGENCY NAME(S) AND ADDRESS(ES)

U.S. Army Research Office
P.O. Box 12211
Research Triangle Park, NC 27709-2211

10. SPONSOR/MONITOR'S ACRONYM(S)
ARO

11. SPONSOR/MONITOR'S REPORT NUMBER(S)
58161-CH-MUR.16

12. DISTRIBUTION AVAILIBILITY STATEMENT

Approved for public release; distribution is unlimited.

13. SUPPLEMENTARY NOTES

The views, opinions and/or findings contained in this report are those of the author(s) and should not contrued as an official Department of the Army position, policy or decision, unless so designated by other documentation.

14. ABSTRACT

An alkaline exchange membrane (AEM) based on an aminated trimethyl poly(phenylene) is studied in detail. This article reports hydroxide ion conductivity through an in situ method that allows for a more accurate measurement. The ionic conductivities of the membrane in bromide and carbonate forms at 90 °C and 95% RH are found to be 13 and 17 mS cm?1 respectively. When exchanged with hydroxide, conductivity improved to 86 mS cm?1 under the same experimental conditions. The effect of relative humidity on water uptake and the SAXS patterns of the AEM

15. SUBJECT TERMS

ionomer;polyaromatics;diffusion;SAXS;alkaline exchange membrane;fuel cell;anion conductivity;anion diffusion

16. SECURITY CLASSIFICATION OF:			17. LIMITATION OF ABSTRACT	15. NUMBER OF PAGES	19a. NAME OF RESPONSIBLE PERSON
a. REPORT	b. ABSTRACT	c. THIS PAGE			Andrew Herring
UU	UU	UU	UU		19b. TELEPHONE NUMBER: 303-384-2082

Report Title

Understanding anion transport in an aminated trimethyl polyphenylene with high anionic conductivity

ABSTRACT

An alkaline exchange membrane (AEM) based on an aminated trimethyl poly(phenylene) is studied in detail. This article reports hydroxide ion conductivity through an in situ method that allows for a more accurate measurement. The ionic conductivities of the membrane in bromide and carbonate forms at 90 °C and 95% RH are found to be 13 and 17 mS cm?1 respectively. When exchanged with hydroxide, conductivity improved to 86 mS cm?1 under the same experimental conditions. The effect of relative humidity on water uptake and the SAXS patterns of the AEM membranes were investigated. SAXS analysis revealed a rigid aromatic structure of the AEM membrane with no microphase separation. The synthesized AEM is shown to be mechanically stable as seen from the water uptake and SAXS studies. Diffusion NMR studies demonstrated a steady state long-range diffusion constant, D? of 9.8 × 10?6 cm2 s?1 after 50–100 ms.

REPORT DOCUMENTATION PAGE (SF298)
(Continuation Sheet)

Continuation for Block 13

ARO Report Number 58161.16-CH-MUR
Understanding anion transport in an aminated tr ...

Block 13: Supplementary Note

Approved for public release; distribution is unlimited.

Understanding Anion Transport in an Aminated Trimethyl Polyphenylene with High Anionic Conductivity

Rajeswari Janarthanan,[1] James L. Horan,[1] Benjamin R. Caire,[1] Zachary C. Ziegler,[1] Yuan Yang,[2] Xiaobing Zuo,[3] Matthew W. Liberatore,[1] Michael R. Hibbs,[4] Andrew M. Herring[1]

[1]Department of Chemical and Biological Engineering, Colorado School of Mines, Golden, Colorado 80401

[2]Department of Chemistry and Geochemistry, Colorado School of Mines, Golden, Colorado 80401

[3]X-Ray Science Division, Argonne National Laboratory, Argonne, Illinois 60439

[4]Department of Materials, Devices, and Energy Technologies, Sandia National Laboratories, Albuquerque, New Mexico 87123

Correspondence to: A. M. Herring (E-mail: aherring@mines.edu)

Received 14 June 2012; revised 15 August 2012; accepted 16 August 2012; published online
DOI: 10.1002/polb.23164

ABSTRACT: An alkaline exchange membrane (AEM) based on an aminated trimethyl poly(phenylene) is studied in detail. This article reports hydroxide ion conductivity through an *in situ* method that allows for a more accurate measurement. The ionic conductivities of the membrane in bromide and carbonate forms at 90 °C and 95% RH are found to be 13 and 17 mS cm^{-1} respectively. When exchanged with hydroxide, conductivity improved to 86 mS cm^{-1} under the same experimental conditions. The effect of relative humidity on water uptake and the SAXS patterns of the AEM membranes were investigated. SAXS analysis revealed a rigid aromatic structure of the AEM membrane with no microphase separation. The synthesized AEM is shown to be mechanically stable as seen from the water uptake and SAXS studies. Diffusion NMR studies demonstrated a steady state long-range diffusion constant, D_∞ of 9.8 $\times$ 10^{-6} cm^2 s^{-1} after 50–100 ms. © 2012 Wiley Periodicals, Inc. J Polym Sci Part B: Polym Phys 000: 000–000, 2012

KEYWORDS: ionomer; polyaromatics; diffusion; SAXS; alkaline exchange membrane; fuel cell; anion conductivity; anion diffusion

INTRODUCTION In recent years, alkaline exchange membrane (AEM) fuel cells are receiving enormous attention due to their potential advantages over proton exchange membrane (PEM) fuel cells such as improved electrode reaction kinetics, the possibility of the use of nonprecious metal catalysts, and advantages in the operation of a direct methanol fuel cell in terms of the direction of electroosmotic drag.[1,2] The AEM at the heart of these fuel cells have received considerable attention due to the challenge in developing a mechanically robust thin film with a stable cation that conducts anions with adequate conductivity for practical applications.[3–5] Several review articles on these issues, and the challenges of using various polymers, have appeared in the recent literature.[6,7] Among the challenges, understanding the transport of anions, water, and the fuel through AEMs is important with relevance to the overall cell performance.[8–13] The degree of phase separation and morphology are known to play key roles in determining measurable properties such as ion conductivity, and diffusion coefficients within all types of ion exchange membranes.[14]

One attractive solution to the problem of obtaining an AEM for fuel cell applications are functionalized polyphenylenes. Thermally and chemically robust, high molecular weight sulfonated poly(phenylene) ionomers prepared by a Diels-Alder reaction and with high proton conductivity have been demonstrated for PEM fuel cells.[15–17] Based on the previous success with these materials, an AEM based on the same poly(phenylene) backbone and with benzyltrimethylammonium cationic groups was also prepared.[18,19] The AEMs based on these aminated trimethyl poly(phenylene) (ATMPP) homopolymers and copolymers were characterized by conductivity and water uptake. It was demonstrated that ATMPPs have good stability in NaOH, a hydroxide ion conductivity of 51 mS cm^{-1} at 30 °C, measured in ambient air, and liquid water uptake up to 122% for the ATMPP polymer with an IEC of 1.57 meq g^{-1}.

Intrigued by the possibilities of the ATMPP membranes we decided to characterize these materials further in detail to understand fully their high anionic conductivities. One of the inherent difficulties with studying AEMs is that in their hydroxide form they rapidly react with ambient CO_2 to form carbonate and bicarbonate.[20] So not only must the relative humidity (RH), and temperature be controlled, but also CO_2 must be excluded or added in order for transport measurements to be interpretable and attributable to a specific anion. Here, we describe the use of an *in situ* hydroxide ion

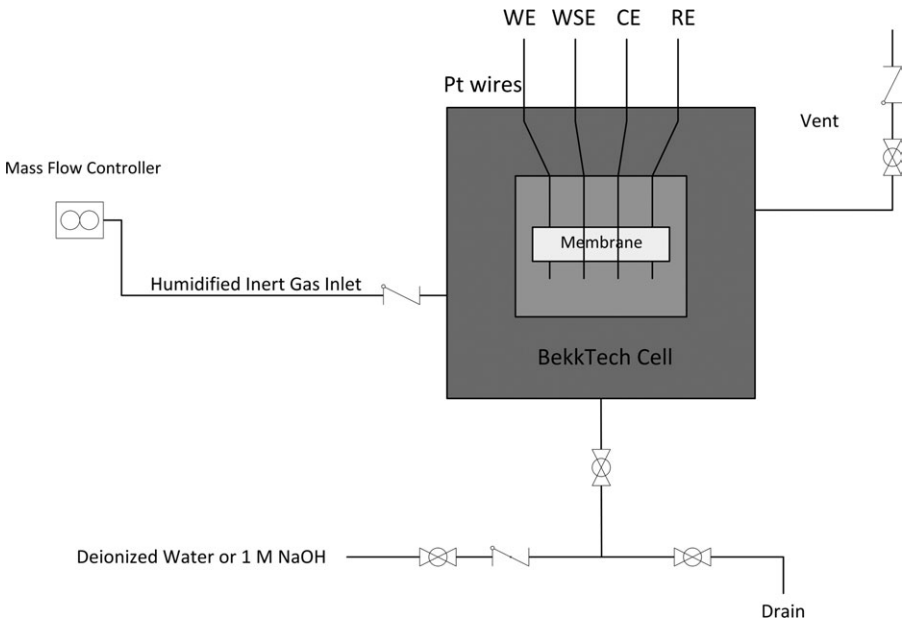

FIGURE 1 A diagram of a modified Bekktech conductivity cell for hydroxide conductivity measurement (WE, Working electrode; WSE, Working sense electrode; RE, Reference electrode; CE, Counter electrode).

exchange conductivity cell that allows us to exchange hydroxide ions in an inert atmosphere, resulting in more accurate hydroxide ion conductivity measurements. We also describe a method for measuring IEC by ^{1}HNMR, which gives results that are much more closely aligned with the predicted values than those previously reported. The transport data is further correlated with diffusion measurements from pulse field gradient spin echo (PFGSE) NMR, water swelling from dynamic vapor sorption (DVS), and morphological information from SAXS.

EXPERIMENTAL

Materials

ATMPPs were fabricated by a procedure previously reported.[18,19]

Ion Exchange Capacity

Ion exchange capacity (IEC) was measured using a back titration technique that has been previously described.[21] IEC was also measured by 1HNMR spectroscopy of ~5% solutions of ATMPP in DMF-d_7 at 100 °C. An explanation of the peak assignments follows in the discussion. A Bruker AVANCEIII NMR spectrometer operating at a ^{1}H frequency of 500 MHz was used for these measurements.

Dynamic Vapor Sorption

A DVS-advantage instrument from Surface Measurement Systems (NA) was used to study water uptake of membranes. In a DVS study, measurement of water vapor uptake and loss of vapor by the membrane is examined gravimetrically. First, the membrane is dried for 60 min at 60 °C and 0% RH to obtain the dry mass. Following this, RH is increased gradually in four steps to reach a maximum of 90% RH. At each step, the membrane was allowed to equilibrate at a particular RH for 60 min.

Small Angle X-ray Scattering

Small angle X-ray scattering (SAXS) measurements were taken on beamline 12 ID-B at the Advanced Photon Source located at Argonne National Laboratory, Argonne, IL. The beam energy was 12 keV and the sample to detector distance was 2000 mm. The 2D scatter was radially integrated providing plots of intensity versus the scattering vector q. The intensity units are arbitrary. The incoming X-ray wavelength (λ) was 1 ± 0.05 Å for all samples. Scattering was collected in a q range of 0.006–0.7 Å^{-1} at an exposure time of 1 s. The measurements were taken in a custom built humidity oven at 60°C from wet to dry conditions (95, 75, 50, and 25% RH).[22] The Membrane in bromide form was exchanged to carbonate form by soaking in sodium carbonate solution.

Conductivity

To measure hydroxide ion conductivity in the absence of carbon dioxide, a BekkTech conductivity cell was modified by having the fuel cell hardware replaced with stainless steel endplates (Fig. 1). The films were soaked in 1 M NaOH solution followed by rinsing with degassed deionized water until the rinsed water had a neutral pH. The system was purged with UHP N_2 each time the cell was emptied. A check valve on the vent and positive pressure on the cell from the UHP N_2 ensured that no outside gas was allowed into the cell across the duration of the conductivity test. Conductivity was measured once the membrane is converted to hydroxide form after thorough rinsing in D.I. water. Bromide ion conductivity was also measured in a Bekktech conductivity cell. However, the carbonate ion conductivity is measured by an *ex situ* method in which a Test Equity environmental chamber is employed to control the temperature and RH. Conductivities were measured using AC impendence spectroscopy

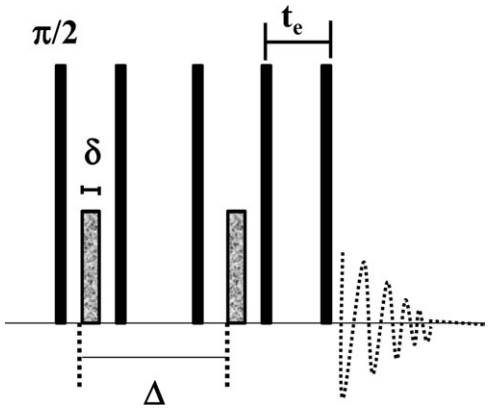

FIGURE 2 A nine interval stimulated echo pulse sequence employed to measure time-dependent self-diffusion on diffusion time, $\Delta_{eff,}$ from 10 to 100 ms.

via a four-electrode conductivity cell across varying temperature and humidity. Conductivity, σ, was calculated using the equation, $\sigma = \frac{l}{R*t*w}$, where l is the distance between the electrodes, t and w are the thickness and width of the membrane, respectively, and R is the resistance from impedance spectra.

PFGSE NMR

A Bruker AVANCEIII NMR spectrometer and a wide bore Magnex Magnet operating at a ^{1}H frequency of 400 MHz were used. Proton diffusion measurements were made using a 5 mm Bruker single-axis DIFF60L Z-diffusion probe. A pulsed field gradient stimulated echo (PFGSTE) block was used to encode diffusive displacements and a longitudinal eddy delay before the acquisition was applied until the effects of the eddy currents have dissipated (Fig. 2).[23,24] The 90° pulse length was on the order of 5.0 μs. Typical parameters at 25 °C were Gz = 0 − 128 G cm^{-1}, incremented in 16 steps, δ = 1 ms, Δ = 10 − 100 ms, and eddy current delay (t_e) of 4 ms following the gradient pulses.

In practice, $E_{(g,2\tau)}$ is measured as a function of g and fit to the expression:[25]

$$E_{(g,2\tau)} = E_{(0,2\tau)} \exp\left(-\gamma^2 D g^2 \delta^2 \left\{\left(\Delta - \frac{\delta}{3}\right)\right\}\right) \qquad (1)$$

where γ is the gyromagnetic ratio of the proton (or the diffusing species being measured), D is the diffusion coefficient, g is the gradient constant, δ is the gradient pulse duration, and Δ is the time between gradient pulses. The preexponential factor $E_{(0,2\tau)}$ is proportional to the number of proton nuclei diffusing with diffusion coefficient D. The effective spin observation time between gradient pulses ($\Delta_{eff} = \Delta - \delta/3$) takes into account the time loss of spin behavior due to the duration of the gradient pulse.

RESULTS AND DISCUSSION

To describe fully, the physical chemistry of these materials we first had to resolve some previously unresolved issues. In work previously describing ATMPP, it was noted that the

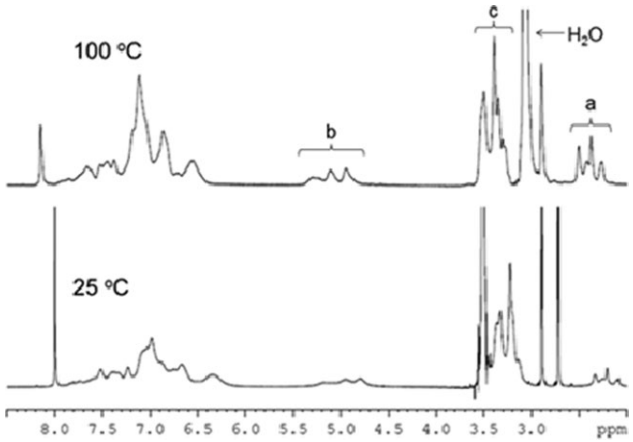

FIGURE 3 ^{1}HNMR spectra of ATMPP at 25 °C and 100 °C.

IEC, which was measured using a back titration method, was always significantly lower than the theoretical IEC predicted from the number of functional groups on the parent polymer (as determined by ^{1}HNMR spectroscopy).[18] Typically, the titration-measured IECs were 55–75% of the theoretical IEC. It was speculated that this difference was because some of the functional groups in the parent polymer were not converted to benzyl trimethylammonium (BTMA) groups. More recently, we have been able to measure the IEC of ATMPP by ^{1}HNMR at an elevated temperature, which allows for precise integration of the requisite peaks. Figure 3 shows the ^{1}HNMR spectra of ATMPP in DMF-d_7 at 25 and 100 °C and it is clear that at the higher temperature, overlap of the large water peak with peak c (N—CH_3) is avoided. All the peaks of interest in Figure 3(a–c) appear as groups of peaks because of the irregularity of the polymer backbone and because of the random distribution of BTMA groups on each repeat unit. To calculate the IEC, the area ratio of peak c to peak b (Ar—CH_2—N) is first confirmed to be 9:2. Then the relative areas of a (Ar—CH_3) and c are used to calculate the average number of BTMA groups per repeat unit, the average formula weight of each repeat unit, and finally the IEC. Table 1 lists the results for several different batches of ATMPP and it is clear that the NMR-measured IECs are in very good agreement with the theoretical IECs. Thus, it appears that all of the functional groups in the parent polymer are converted to BTMAs during the quaternization step. The titration-measured IECs must be low because of a systemic error during the titration itself; possibly incomplete ion exchange,

TABLE 1 IEC Values for Several ATMPP Samples

	IEC (meq g^{-1}) (OH$^-$ form)		
	Theoretical	Titration	NMR
$ATMPP_1$	1.91	1.47	1.89
$ATMPP_2$	2.10	1.58	2.05
$ATMPP_3$	2.18	1.75	2.11
$ATMPP_4$	2.40	1.81	2.43
$ATMPP_5$	2.65	1.97	2.67

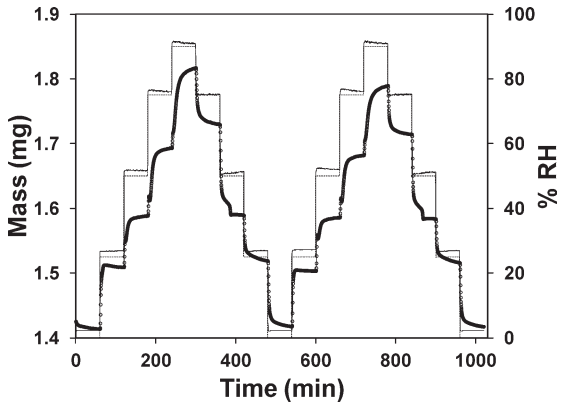

FIGURE 4 DVS profile for $ATMPP_4$ membrane as a function of RH at 60 °C, circles: mass, solid line: set %RH, and dotted line: measured %RH.

incomplete drying, or removal of water-soluble high IEC oligomers. Alternatively, as we have considerable experience of this technique some of the cationic groups are not accessible to facile exchange due to the unique nature of the polymer. Because of this uncertainty, all reported IECs for ATMPP samples used in this study were determined using the NMR method.

The IEC of the membranes can influence the water uptake, swelling behavior, and conductivity. The Water uptake of AEMs can have a significant effect on the anionic conductivity and the films mechanical properties. For practical operation, it would be desirable to have enough water molecules that facilitate hydroxide ion transport and stability, but, not an excess amount of water that would reduce the mechanical strength of the membranes and lead to excessive swelling. Water vapor uptake of the membranes was measured by DVS. A typical water sorption isotherm measured at 60 °C is shown in Figure 4. The trace shows that equilibrium was reached at all RHs except the higher one, and even here the rate of water uptake is close to zero at the end of the step. The sorption profile traces the uptake when the humidity was increased from 0 to 95% RH. The desorption profile from 95% RH down to 0% RH measures the loss of vapor during each change in % RH.

Water uptake at a specific % RH is calculated from eq 2,

$$\text{Wateruptake}_{\text{RH}}\% = \frac{m_{\text{w}} - m_{\text{d}}}{m_{\text{d}}} * 100 \qquad (2)$$

where m_{w} refers to the equilibrium mass at a specific %RH and m_{d} is the dry mass of the membrane.

The water content, λ_{RH}, the number of water molecules at a specific RH is calculated from eq 3,

$$\lambda_{\text{RH}} = \frac{\text{Wateruptake}_{\text{RH}}}{\text{IEC} * \text{MW}_{\text{water}}} \qquad (3)$$

where, MW_{water} is the molecular weight of water = 18 g mol^{-1}.

The second cycle in Figure 4 shows a loss in water uptake of ~5% when compared with first cycle. This could be due to partial decomposition of quaternary ammonium group in the membrane during the drying part of the cycle, or simply that the membrane irreversibly loses water when subjected to multiple drying cycles. A comparison of the IR spectra of the film before and after the DVS measurement showed no obvious changes.

Water uptake and water content of membranes with two IEC values as a function of relative RH at 60 °C are shown in Figures 5(a, b), respectively, after 1 h of equilibration at each %RH. The water uptake of both membranes is similar, increasing as the RH is increased. Water uptake in these membranes is significantly lower than the sulfonated analogues. A sulfonated polyphenylene analogue (2 meq g^{-1}) was found to exhibit 137% liquid water uptake that corresponds to 30 water molecules.[15] While liquid water uptake is always greater than water vapor uptake,[26] the difference in the water uptake can be attributed to the lower solubility of the cationic functional groups as well as the fact that hydroxide is generally coordinated by 3–4 waters only.[27] This indicates a low swelling and good dimensional stability of the ATMPP membranes. The water content of the membranes, derived from the water uptake and IEC of the membranes, shows an increasing trend with RH. Water uptake of 6.6 and 27.2% for the low IEC membrane (2.43 meq g^{-1}) correspond to 1.5 and 6.2 water molecules per ATMPP unit.

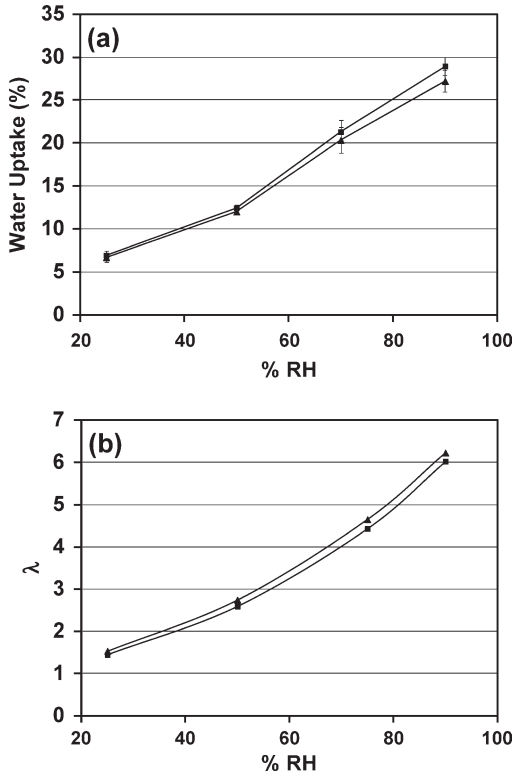

FIGURE 5 (a) Water uptake and (b) Water content of the $ATMPP_4$ (▲) and $ATMPP_5$ (■) derived from DVS measurements at an equilibration time of 1 h at each % RH.

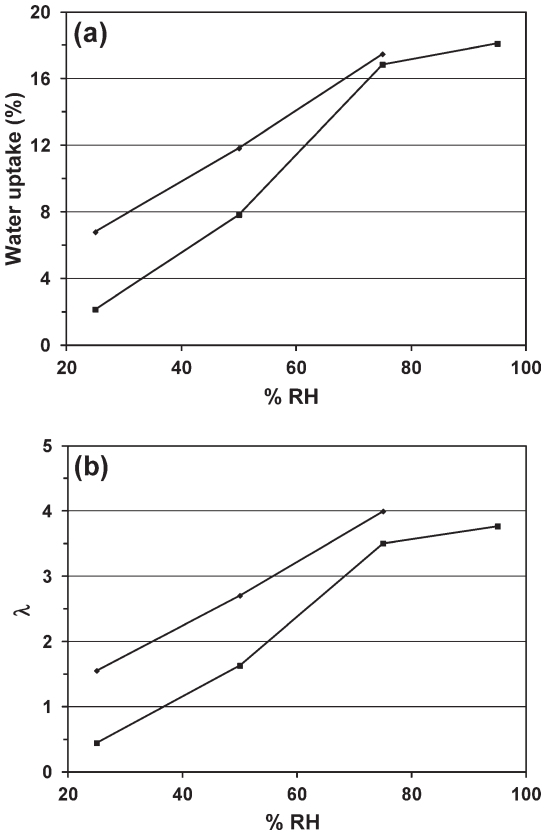

FIGURE 6 (a) Water uptake and (b) Water content of the $ATMPP_4$ (◆) and $ATMPP_5$ 2.67 (■) derived from DVS measurements at an equilibration time of 20 min at each % RH.

A slight increase in the IEC of the membrane (2.67 meq g^{-1}) increases the number of water molecules slightly, resulting in 1.4 and 6.0 per ATMPP unit. At the upper end the films, therefore, contain two excess water molecules.

SAXS was measured on the films for shorter equilibration times, due to scheduling a large number of samples during our beam time. The water uptake of the membranes in bromide forms after only 20 min (SAXS equilibration time) is shown in Figure 6(a, b). Unlike in the 1 h water uptake study above, in this experiment, the RH was reduced from a fully hydrated state to 25% RH. Water uptake and the corresponding water content of low IEC membrane are slightly greater than the high IEC membrane. We could not measure water uptake at 95% RH for $ATMPP_4$ as the membrane did not achieve an equilibrium mass within the short time frame.

The SAXS patterns of the $ATMPP_4$ membrane in bromide form as a function of RH at 60 °C is shown in Figure 7. The peak around 0.4 Å corresponds to the Kapton™ windows in the oven. The SAXS data for the membrane showed no scattering peaks, thus making it difficult to understand the microdomain structure. The ATMPP ionomer is composed of the poly (phenylene) aromatic backbone and BTMA ionic groups (Fig. 8). No scattering peak was observed for the $ATMPP_4$ ionomer from 25 to 75% RH indicating almost no

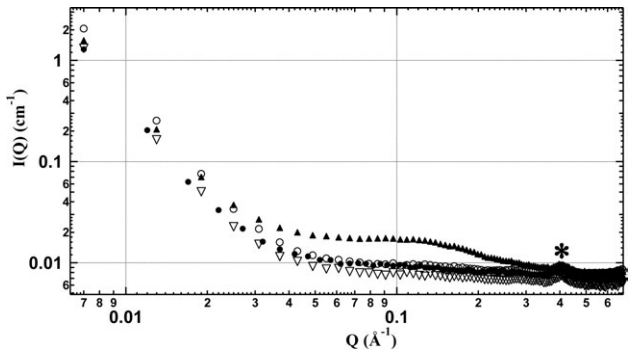

FIGURE 7 SAXS patterns of the $ATMPP_4$-Br^- at 60 °C as a function of RH (▲–95% RH; ▽–75% RH; ▲–50% RH; ●–25% RH; *–Kapton peak).

microphase separation in the polymer. Under fully hydrated condition, at 95% RH, the membrane swells to show a peak at q value of ~0.124 $Å^{-1}$, corresponding to 50 Å d-spacing, which can be assigned to the swollen hydrophilic ionomer. This is larger than the hydrated sulfonated analogue, which showed a peak upon hydration with a dimension of 32 Å.[28] At low q range (0.007–0.017 $Å^{-1}$) an upturn in intensity is observed, which has been attributed to the presence of microvoids or heterogeneous distribution of clusters.[29,30] SANS study of sulfonated polyphenylene showed a similar high intensity scattering for both dry and hydrated membranes due to the large domains.[28] In the low angle region, between 0.07 and 0.017 $Å^{-1}$, membranes were found to exhibit power law decay, $I(q) = q^{-\alpha}$, with a slope of −3.4 at all conditions. Whereas, at the intermediate q region, between 0.018 and 0.035 $Å^{-1}$, 95% RH membrane has a slope (−1.7) different from all other membranes (−2.3), suggesting a structural rearrangement from randomly branched polymer to a linear swollen polymer upon full hydration.[31,32] The crossover of slopes from low angle to intermediate region occurs at $q = 0.02$ $Å^{-1}$, which corresponds to a d-spacing of 314 Å. In a similar SANS study of the sulfonated analogue of the polymer, crossover point is referred as the molecular dimensions.[28]

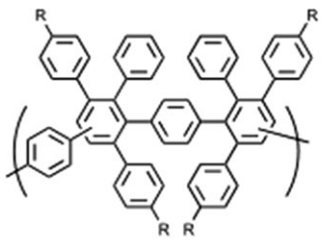

ATMPP **R = CH_3 or $\overset{\oplus}{C}H_2N(CH_3)_3$**

for 7-138-E, 43% of the R groups are methyls
for 7-99-B, 28% of the R groups are methyls

FIGURE 8 Structure of ATMPP.

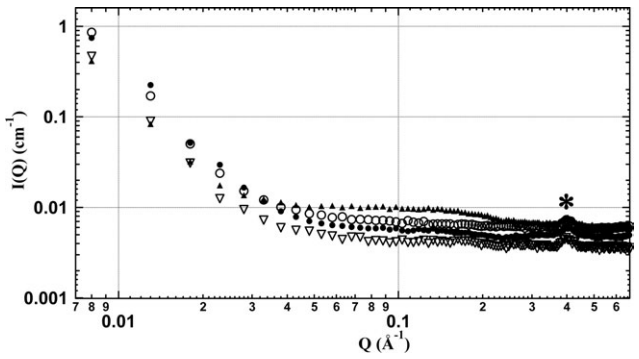

FIGURE 9 SAXS patterns of the ATMPP$_4$-CO_3^{2-} at 60 °C as a function of RH (▲–95% RH; ▽–75% RH; ●–50% RH; ▲–25% RH; *–Kapton peak).

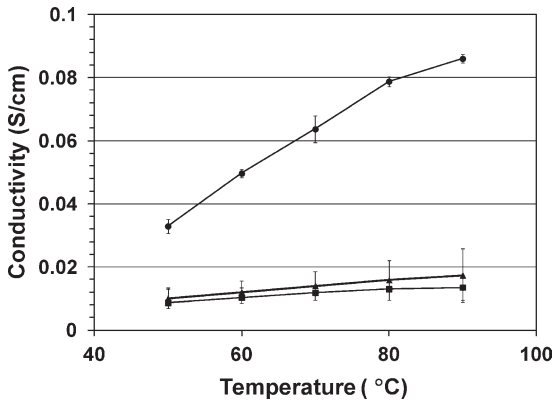

FIGURE 10 Conductivity of ATMPP$_4$ membrane in its bromide (■), carbonate (▲), and hydroxide (●) forms as a function of temperature at 95% RH.

ATMPP$_4$ in carbonate form too exhibit different slope values as a function of RH (Fig. 9). All membranes show an upturn in intensity at low intermediate q region between 0.007 and 0.017 Å^{-1}, with different slopes as described in Table 2. Slopes were seen to change as a function of RH in the intermediate region, 0.016 – 0.021 Å^{-1} as well (Table 2). The swelling in the pattern at high q region, 0.036 – 0.225 Å^{-1} for the 95% RH membrane is due to the water present in the free volume upon full hydration.

SAXS measurements reveal no change in the microstructure due to the rigid aromatic backbone of the ATMPP. However, the change in RH has a small effect on the structure as evident from the change in slopes at different q regions. Overall, the lack of swelling in these films is unsurprising as the DVS measurement suggests that only enough water to coordinate the anion has entered the material.

Figure 10 exhibits the Br^-, OH^-, and CO_3^{2-} ion conductivities of the ATMPP$_4$ at 95% RH as a function of temperature. As expected, the conductivity increased over the temperature range tested for all forms of the membrane. When the bromide ion of the membrane is exchanged with hydroxide ion, the conductivity increased rapidly. At 50 °C, the OH^- form showed four times high conductivity when compared to the Br^- form. At 90 °C, the hydroxide ion showed highest conductivity of 86 mS cm^{-1}, ~6.6 times higher than that of bromide form. This value is lower than the proton conductivity of sulfonated polyphenylene membrane, 123 mS cm^{-1}.[15] This response could be due to the variation in the structure as well as the mobility of OH^- and H^+ ions in the aminated and sulfonated polyphenylenes, respectively. The carbonate ion conductivity is significantly lower than the hydroxide ion as expected. Still, the conductivity at 90 °C is 1.28 times higher than bromide ion. Assuming, Arrhenius behavior, activation energies of the membranes are calculated from the equation, $E_a = -\text{slope} \times R$, where R is the gas constant. Activation energies are 29.09, 23.45, and 11.02 kJ mol^{-1} for the carbonate, hydroxide, and bromide forms of the membrane, respectively, at 95% RH. This value for hydroxide and carbonate ion conduction is higher than the lowest activation energies for hydroxyl in AEMs, 15.1 kJ mol^{-1} reported by Varcoe[10] at 100% RH. Interestingly, the E_a for bromide conductivity is much lower.

TABLE 2 SAXS Slope Values Derived from Power Law

Membrane	% RH	Low q region	Intermediate q region
ATMPP4-Br	95	−3.4	−1.7
	75	−3.4	−2.3
	50	−3.4	−2.3
	25	−3.4	−2.3
ATMPP4-CO_3	95	−3.1	Not linear
	75	−3.3	−3.0
	50	Not linear	−3.2
	25	−3.5	−2.6

PFGSE proton diffusion measurements were used to determine the water self-diffusion coefficients (D) in the hydroxide form of the ATMPP. Variable time delay (Δ) between gradient pulses of the PFGSE sequence can be used to determine the effects of tortuous diffusion through ionomer membranes on the measured diffusion coefficient.[33] The relationship between apparent diffusion time (Δ) and spin migration by root mean square displacement (r) for fluid molecules exhibiting unrestricted diffusion undergoing random Brownian motion is shown by the following relationship:[34]

$$r = (2\Delta D)^{0.5} \quad (4)$$

The unrestricted bulk diffusion coefficient (D_0) of water in the membrane is measured with very short time delays between the gradient pulses and thus the spin migration (r) of the diffusing species is smaller than the dimensional regime of the restricting geometry. For short time scales, $D = D_0$. In the case of restricted diffusion in a membrane, as Δ increases, the root mean square displacement increases until the geometric confinement of the heterogeneous media restricts the displacement of spin migration. Once restriction

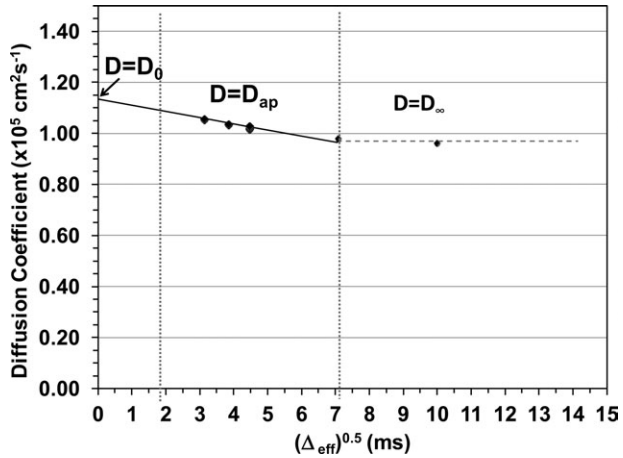

FIGURE 11 Measured self-diffusion coefficients, D (Δ_{eff}) versus the square root of the effective diffusion time, Δ_{eff}.

takes place, the diffusion coefficient decreases with increasing Δ. The root mean square displacement (r) no longer exhibits a linear relationship with the diffusion coefficient. For example, within a spherical pore, the apparent diffusion coefficient (D_{ap}) becomes time dependent as the diffusing species interacts with the pore wall.[35,36] At very long diffusion times, the full effect of tortuous diffusion in the membrane causes the diffusion constant to reach an average steady state (D_∞).[37,38]

Very little evidence of tortuous diffusion was found in the ATMPP-OH membrane at room temperature. By varying the time between gradient pulses (Δ) in the pulse sequence, the linear dimension of the diffusing particle was probed. The diffusion time (Δ) was varied from 10 to 100 ms to probe various diffusion length scales in an effort to look for any morphological barriers that may result in tortuous diffusion behavior. For very short diffusion times, the resulting diffusion coefficient is time dependent with maximum mean square displacement of the diffusing species less than the confined restricting volume.[34] We did not observe this behavior with the short Δ values we tested, so the actual value of D_0 must lie in an observation range $<$10 ms. We were unable to measure diffusion values for observation times $<$10 ms, but, we can extrapolate our data for short observation times on a plot of D versus $(\Delta_{eff})^{0.5}$ (Fig. 11) using the Mitra equation to predict the value for D_0:[34–39]

$$D(\Delta_{eff}) = D_0\left[1 - \frac{4}{9\sqrt{\pi}}\frac{S}{V}\sqrt{D_0\Delta_{eff}}\right] \quad (5)$$

where S/V is the surface to volume ratio of pore space. In the ATMPP-OH membrane, the D_o value extrapolates to a y-intercept value of 1.1×10^{-5} cm^2 s^{-1}. At diffusion times between 10 and 50 ms, the echo attenuation and the echo amplitude depends more on the confining geometry determined by morphological barriers than on diffusion time ($D = D_{ap}$). Therefore, D_{ap} values range between 1.1×10^{-5} cm^2 s^{-1} and 9.9×10^{-6} cm^2 s^{-1}. The time dependent decrease in diffusion constants over this range is an indication of tortuous diffusion, yet it is evident that the degree of restriction is very limited due to the minor difference in diffusion constant values over this range before we observe a steady state value. At diffusion times between 50 and 100 ms, a steady state value for D_∞ of 9.8×10^{-6} cm^2 s^{-1} is reached.

CONCLUSIONS

In this study, aromatic anion exchange membranes based on aminated poly(phenylene) homopolymers were synthesized and investigated in both bromide and hydroxide forms. Low water uptake and water content values calculated from DVS studies revealed good mechanical stability of the membranes. These values were observed to decrease when the experiments were carried out in a short time to match the SAXS experimental time duration. From SAXS, the polymer exhibited structural rearrangement between low and intermediate q regions, when the membranes were subjected to different RH. However, there was no specific feature observed due to the ionomer, indicating poor microphase separation. This can be attributed to the rigid aromatic backbone of the polymer. To avoid exchange of hydroxide ions to carbonate or bicarbonate ions when exposed to air, we have performed in-situ hydroxide ion conductivity measurement. The OH^- conductivity of the membrane was 86 mS cm^{-1}, which is 6.6 times higher than its bromide form. We have also described a method for determining IEC by NMR, which indicates that the formation of BTMA cations during the synthesis of ATMPP in nearly quantitative, contrary to our prior report. This ATMPP membrane with a low water content and high conductivity demonstrates a promising AEM for alkaline fuel cells applications.

ACKNOWLEDGMENTS

This work was supported by a LDRD grant from Sandia National Laboratories and in part by the ARO through a MURI award, W911NF-10-1-0520. Use of the Advanced Photon Source was supported by the U.S. Department of Energy, Office of Science, Office of Basic Energy Sciences, under Contract No. DE-AC02-06CH11357.

REFERENCES AND NOTES

1 Lu, S.; Pan, J.; Huang, A.; Zhuang, L.; Lu, J. *Proc. Natl. Acad. Sci. USA* **2008,** *105*, 20611–20614.

2 Gulzow, E. *J. Power Sources* **1996,** *61*, 99–104.

3 Matsui, K.; Tobita, E.; Sugimoto, K.; Kondo, K.; Seita, T.; Akimoto, A. *J. Appl. Polym. Sci.* **1986,** *32*, 4137–4143.

4 Gu, S.; Cai, R.; Luo, T.; Chen, Z.; Sun, M.; Liu, Y.; He, G.; Yan, Y. *Angew. Chem. Int. Ed.* **2009,** *48*, 6499–6502.

5 Tomoi, M.; Yamaguchi, K.; Ando, R.; Kantake, Y.; Aosaki, Y.; Kubota, H. *J. Appl. Polym. Sci.* **1997,** *64*, 1161–1167.

6 Varcoe, J. R.; Slade, R. C. T. *Fuel Cells* **2005,** *5*, 187–200.

7 Merle, G.; Wessling, M.; Nijmeijer, K. *J. Membr. Sci.* **2011,** *377*, 1–35.

8 Mamlouk, M.; Wang, X.; Scott, K.; Horsfall, J. A.; Williams, C. *Proc. IME. J. Power Energy* **2011,** *225*, 152–160.

9 Robertson, N. J.; Kostalik IV, H. A.; Clark, T. J.; Mutolo, P. F.; Abruna, H. D.; Coates, G. W. *J. Am. Chem. Soc.* **2010,** *132*, 3400–3404.

10 Varcoe, J. R. *Phys. Chem. Chem. Phys.* **2007,** *9*, 1479–1486.

11 Zhang, H.; Ohashi, H.; Tamaki, T.; Yamaguchi, T. *J. Phys. Chem. C* **2012,** *116*, 7650–7657.

12 Yamanaka, T.; Takeguchi, T.; Takahashi, H. *J. Electrochem. Soc.* **2009,** *156*, B831–B835.

13 Li, Y. S.; Zhao, T. S.; Yang, W. W. *Int. J. Hydrogen Energy* **2010,** *35*, 5656–5665.

14 Jing, P.; Shanfu, L.; Yan, L.; Aibin, H.; Lin, Z.; Juntao, L. *Adv. Funct. Mater.* **2010,** *20*, 312–319.

15 Fujimoto, Cy H.; Hickner, M. A.; Cornelius, C. J.; Loy, D. A. *Macromolecules* **2005,** *38*, 5010–5016.

16 Hickner, M. A.; Fujimoto, Cy H.; Cornelius, C. *J. Polymer* **2006,** *47*, 4238–4244.

17 Stanis, R. J.; Yaklin, M. A.; Cornelius, C. J.; Takatera, T.; Umemoto, A.; Ambrosini, A.; Fujimoto, Cy H. *J. Power Sources* **2010,** *195*, 104–110.

18 Hibbs, M. R.; Fujimoto, Cy H.; Cornelius, C. *J. Macromolecules* **2009,** *42*, 8316–8321.

19 Hibbs, M. R.; Cornelius, C. J.; Fujimoto, Cy H. U.S. Patent 7,888, 397, February 15, **2011.**

20 Yan, J.; Hickner, M. A. *Macromolecules* **2010,** *43*, 2349–2356.

21 Hibbs, M. R.; Hickner, M. A.; Alam, T. M.; McIntyre, S. K.; Fujimoto, Cy H.; Cornelius, C. J. *Chem. Mater.* **2008,** *20*, 2566–2573.

22 Schlichting, G. J.; Horan, J. L.; Jessop, J. D.; Nelson, S. E.; Seifert, S.; Yang, Y.; Herring, A. M. *Macromolecules* **2012,** *45*, 3874–3882.

23 Cotts, R. M.; Hoch, M. J. R.; Sun, T.; Markert, J. T. *J. Magn. Reson. (1969)* **1989,** *83*, 252–266.

24 Tanner, J. E. *J. Chem. Phys.* **1970,** *52*, 2523–2526.

25 Strejskal, E. O.; Tanner, J. E. *J. Chem. Phys.* **1965,** *42*, 288.

26 Kusoglu, A.; Modestino, M. A.; Hexemer, A.; Segalman, R. A.; Weber, A. Z. *ACS Macro. Lett.* **2012,** *1*, 33–36.

27 Tuckerman, M. E.; Marx, D.; Parrinello, M. *Nature* **2002,** *417*, 925–929.

28 He, L.; Fujimoto, Cy H.; Cornelius, C. J.; Perahia, D. *Macromolecules* **2009,** *42*, 7084–7090.

29 Gebel, G.; Diat, O. *Fuel Cells* **2005,** *5*, 261–276.

30 Yarusso, D. J.; Cooper, S. L. *Macromolecules* **1983,** *16,* 1871.

31 Beaucage, G. *J. Appl. Crystallogr.* **1995,** *28*, 717–728.

32 Beaucage, G. *J. Appl. Crystallogr.* **1996,** *29*, 134–146.

33 Zhang, J.; Giotto, M. V.; Wen, W. Y.; Jones, A. A. *J. Membr. Sci.* **2006,** *269*, 118–125.

34 Ohkubo, T.; Kidena, K.; Ohira, A. *Macromolecules* **2008,** *41*, 8688–8693.

35 Mitra, P. P.; Sen, P. N.; Schwartz, L. M.; Le Doussal, P. *Phys. Rev. Lett.* **1992,** *68*, 3555–3558.

36 Wende, C.; Schonhoff, M. *Langmuir* **2010,** *26*, 8352–8357.

37 Guillermo, A.; Bardet, M. *Anal. Chem.* **2007,** *79*, 6718–6726.

38 Rollet, A. L.; Blachot, J. F.; Delville, A.; Diat, O.; Guillermo, A.; Porion, P.; Rubatat, L.; Gebel, G. *Eur. Phys. J E. Soft Matter.* **2003,** *12*, 131–134.

39 Rollet, A. L.; Simonin, J. P.; Turq, P.; Gebel, G.; Kahn, R.; Vandais, A.; Noel, J. P.; Malveau, C.; Canet, D. *J. Phys. Chem. B* **2001,** *105*, 4503–4509.